Materials and Design 197 (2021) 109215

Contents lists available at ScienceDirect

Materials and Design

journal homepage: www.elsevier.com/locate/matdes

Machining-induced thermal damage in cortical bone: Necrosis and micro-mechanical integrity

Jose A. Robles-Linares [a], Dragos Axinte [a,b,*], Zhirong Liao [a,**], Andres Gameros [a]

[a] Machining and Condition Monitoring Group, Faculty of Engineering, University of Nottingham, Nottingham NG7 2RD, UK
[b] Faculty of Science and Engineering, University of Nottingham Ningbo China, Ningbo, China

HIGHLIGHTS

- Machining-induced damage in cortical bone was investigated with histology and micro-pillar compression tests.
- In high temperature drilling, micro-mechanical damage occurs as a brittle and weak layer deeper than the necrotic region.
- In low temperature drilling, micro-mechanical damage is inexistent and only necrotic damage arises.

GRAPHICAL ABSTRACT

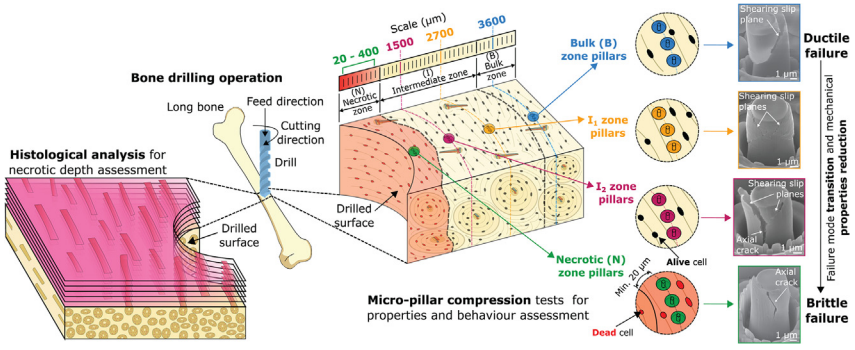

ARTICLE INFO

Article history:
Received 6 July 2020
Received in revised form 4 September 2020
Accepted 6 October 2020
Available online 10 October 2020

Keywords:
Micro-mechanics
Micro-pillar compression
Bone failure mechanism
Histology
Necrosis
Bone cutting

ABSTRACT

In bone cutting, the tissue is exposed to necrosis due to temperature elevation, which can significantly influence postoperative results in orthopaedic surgeries. This damage is usually revealed through histological analysis to show the necrotic extent; however, this technique does not capture mechanical damage, which is essential for a full material integrity assessment. Here, with micro-mechanics, it is demonstrated that machining-induced damage in bone extends beyond the necrotic region. Drilling with different conditions was performed on ex-vivo bovine cortical bone, inducing different damage degrees. Micro-pillar compression tests were performed in the machined sub-surface to identify changes in properties and failure modes caused by drilling. It was revealed that at high cutting temperatures, the bone near the machined surface suffers from lower modulus (−42%), strength (−41%) and brittle behaviour, whereas the bulk bone remains undamaged with pristine properties and ductile behaviour. Histology was also performed to evaluate necrosis and, surprisingly, it was found that the brittle and weaker bone layer is more than three times larger when compared to the necrotic layer, clearly showing that the drilling thermo-mechanical effect could affect not only biologically, but also micro-mechanically. Consequently, these results reveal another kind of bone damage that has so far been neglected.

1. Introduction

From an engineering standpoint, cortical bone is a tissue that microstructurally consists of unidirectional fibres (i.e. osteons) that run through the principal loading direction (i.e. bone's long axis) [1]. These are immersed in a matrix (i.e. interstitial lamellae) comprised of pieces of older osteons that were partly resorbed during the remodelling process of bone [2]. Moreover, it possesses two porosity systems

* Corresponding author at: Machining and Condition Monitoring Group, Faculty of Engineering, University of Nottingham, Nottingham NG7 2RD, UK; Faculty of Science and Engineering, University of Nottingham Ningbo China, Ningbo, China.
** Corresponding author.
E-mail addresses: Dragos.Axinte@nottingham.ac.uk (D. Axinte), Zhirong.Liao@nottingham.ac.uk (Z. Liao).

https://doi.org/10.1016/j.matdes.2020.109215

that contain the transcortical and longitudinal blood, nerve and interstitial fluid supplies [3]. These arrangements yield a complicated composite structure [4] as they provide an intricate hierarchical organisation at the macro-, micro- and nano-scales [5]. This translates into unique anisotropic properties that make bone a complex material for analysis in terms of damage and mechanical performance (e.g. behaviour under cutting [6,7]), particularly when aimed to evaluate machining-induced (i.e. drilling operation) damage. The high cutting temperatures and strains produced by machining can damage the surface of not only engineering materials (e.g. composites [8,9]), but also biological (e.g. tissues [10,11]). Thus, particular attention to machining damage in bone surgery is required.

Furthermore, in-depth understanding of bone damage requires consideration of the biological nature of the bone's cellular structure by means of its three main cell types: osteoclasts, osteoblasts and osteocytes. Osteoclasts and osteoblasts are located on the bone surface and are responsible for the modelling and remodelling process of the bone (e.g. recovery after machining [12] or fracture [13]), while osteocytes are a mature form of osteoblasts that are trapped within the bone inside pits called lacunae [14] and play a major role in monitoring the metabolism and remodelling process [15]. For these cells to perform their vital functions properly and not compromise the bone integrity, they must remain free of damage and below a threshold temperature [14]. Therefore, should tissue necrosis (i.e. cell death) occur in a clinical context (e.g. orthopaedic surgery), it will represent a serious problem for the patient, since the regeneration capacity of the bone will be partially or permanently hindered [16,17].

Bone damage (e.g. by machining operation) at the cellular level can compromise the remodelling process with necrosis. Besides being a useful technique for monitoring the regeneration process of bone [18], histology is considered the gold standard for necrosis assessment, since it allows in-situ analysis of its cells [19]. With this technique, the 'alive' or 'dead' states are determined by the appearance of the osteocytes [14]. In 'dead' bone, the lacunae appear empty, implying that when necrosis occurs, the osteocytes disappear from the lacunae [14], as shown in Fig. 1 for the case of machining-induced necrosis.

Histology has been used to evaluate the necrotic depth caused by drilling into bone, revealing that higher cutting speeds and lower feed rates yield higher temperatures near the drilled surface, leading to greater necrotic depths [20,21]. Research on this field shows that most studies aimed at evaluating machining-induced bone damage have focused on finding the relationship of the necrotic depth with different cutting conditions that may occur during surgery (e.g. speeds, temperatures, forces). As a consequence, bone cutting tool design has been tailored to minimise temperature rise [22,23].

Being a material that sustains mechanical loads in the human body, mechanical damage (e.g. mechanical properties changes, failure mechanism shifts) should also be of relevance and employed in parallel with histology for a full material integrity assessment. A promising approach on mechanical damage assessment is micro-mechanics, as it allows for localised (i.e. near the machined surface) material testing [24].

Micro-mechanical testing of bone has been employed since the 1980s with the aim of mapping the elastic properties [25,26] of its different constituents (e.g. osteons [27], trabeculae [28]) and to characterise the bone repair mechanism [29]. Moreover, recent research has raised attention to the post-yield behaviour of the bone structure since there is a ductile-to-brittle failure mechanism transition going from the micro- to the macro-scale, respectively [30]. Micro-indentation and micro-pillar compression are useful techniques for comprehensively evaluating the mechanical behaviour in both the elastic and plastic regions of the material [31,32], and so could be used to evaluate damage [33,34]. Even though these techniques have been used for bone characterisation in dry [25,32] and wet [35,36] conditions, they have not been explored for assessing machining-induced micro-mechanical alterations. Moreover, as opposed to the complex analysis that micro-indentations require, micro-pillar compression allows for a

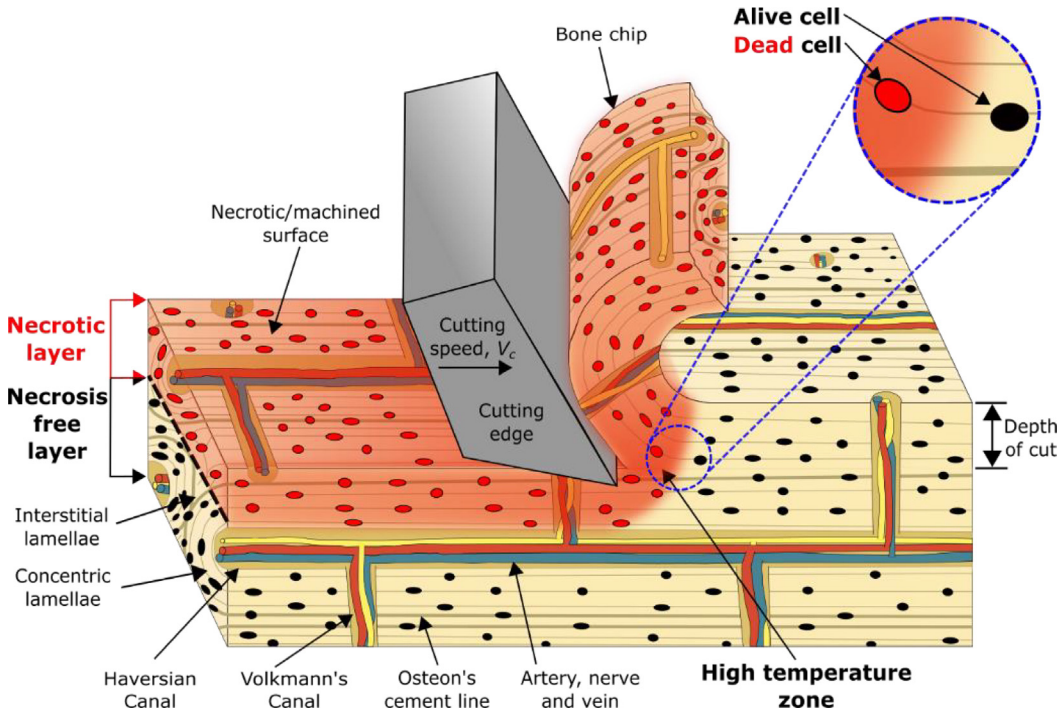

Fig. 1. Schematic of the machining-induced thermal damage in cortical bone, which results in the formation of a layer with necrosis and a damage-free layer. As the cutting edge removes material, it leaves behind a machined surface heated by the dissipation of the cutting energy. This heat propagates deeper into the bone and, if the temperature is high enough (47 °C [39]), it causes osteocyte necrosis (dead cells shown in red colour) and the lacunae to empty. The regions far enough from this heat source (cutting edge) remain with their osteocytes alive and undamaged inside their respective lacunae (represented in black colour). But is there a difference in the micro-mechanical behaviour in the regions with alive and dead cells? (For interpretation of the references to colour in this figure legend, the reader is referred to the web version of this article.)

straightforward analysis that enables understanding of the energy dissipation of the material under both the elastic and plastic domains. Therefore, micro-pillar compression testing is an important micro-mechanics technique that could be employed for damage assessment in bone.

Bone mechanical assessment in this direction has been made focusing on the mechanical behaviour at the macro-scale [37,38] and micro-cracks formation [11], but these have so far failed to successfully capture micro-scale effects in terms of mechanical properties or localised failure mechanisms. However, it is at this micro-level of detail where we can start to understand the true extent of bone damage after machining, from both the micro-mechanical and biological perspectives, allowing evaluation of any implications this could have on the bone's functionality.

Following these propositions, here, we investigate three questions: What are the micro-mechanical characteristics (i.e. modulus of elasticity, compressive yield strength and compressive ultimate strength) and failure mechanisms of cortical bone in areas near and far from a machined surface? How does the micro-mechanical behaviour of the bone change as a function of distance from the machined surface? What is the relationship between the necrotic depth and the micro-mechanical properties? To address these questions, we performed drilling trials in ex-vivo bovine cortical bone under two distinct machining conditions (i.e. low temperature and high temperature) aimed to induce different levels of sub-surface damage. The drilled samples were sectioned and histologically analysed to evaluate the layer of necrotic damage. Scanning Electron Microscopy (SEM) was also employed to capture the macro-damage in the machined surface while micro-pillars were fabricated with a Focused Ion Beam (FIB) milling technique in the drilled sub-surface to conduct micro-mechanics tests with an in-situ SEM method. This paper reports, for the first time, the micro-mechanical characteristics of damaged cortical bone after drilling operations, and the results are complemented with the traditional assessment technique of histology that serves to quantify necrotic damage.

2. Materials and methods

2.1. Sample acquisition and quality

Bovine femur has been used on these investigations as it resembles human bone in the macro- and micro-structural composition, healing capabilities, apparent density, mineral content, elastic modulus and ultimate strength [40,41]. These characteristics make it a suitable human bone model for mechanical and biological testing on both the macro-level (e.g. tensile tests, impact tests) and micro-level (e.g. micro-indentation, micro-pillar compression, histology). Within five hours from the acquisition, samples containing the mid-diaphysis were cut at room temperature under abundant saline solution [42,43] to obtain sections of roughly $50 \times 40 \times 9$ mm^3.

To obtain a flat smooth surface on the samples suitable for micro-testing [44], they were manually ground and polished in a polishing machine (Tegrapol-21, Struers) under abundant saline solution with various SiC grit sizes (200 to 1200), diamond particle suspension (6 to 1 μm) and 0.06 μm colloidal silica, employing fresh saline water rinsing (i.e. ultrasonic bath) after each step [45]. This sample preparation process was used for all the experiments.

The chemical composition of biological specimens can be obtained with Raman spectroscopy [46]; hence this technique was used to validate that the bone was chemically acceptable (i.e. within values stated in literature for healthy bone) to be employed for the experiments. A mapping was performed on the bone in dry condition (48-h air-drying) using a confocal Raman microscope (Horiba LabRAM HR), employing a 785 nm laser excitation wavelength to minimise the fluorescence effect [47], 25 s of acquisition time, grating of 600 lines/mm and a 50× objective with numerical aperture of 0.55. To avoid tissue damage to the microstructure and cells, laser power was maintained below 5 mW [48]. The Raman spectra analysis of 22 different points (example in Fig. 2) resulted in a mineralisation of 12.12 ± 1.50 (average ± std. dev, $n = 22$), a carbonate substitution of 8.19 ± 0.28 ($n = 22$) and a crystallinity of 19.29 ± 0.63 cm^{-1} ($n = 22$), which is in good agreement

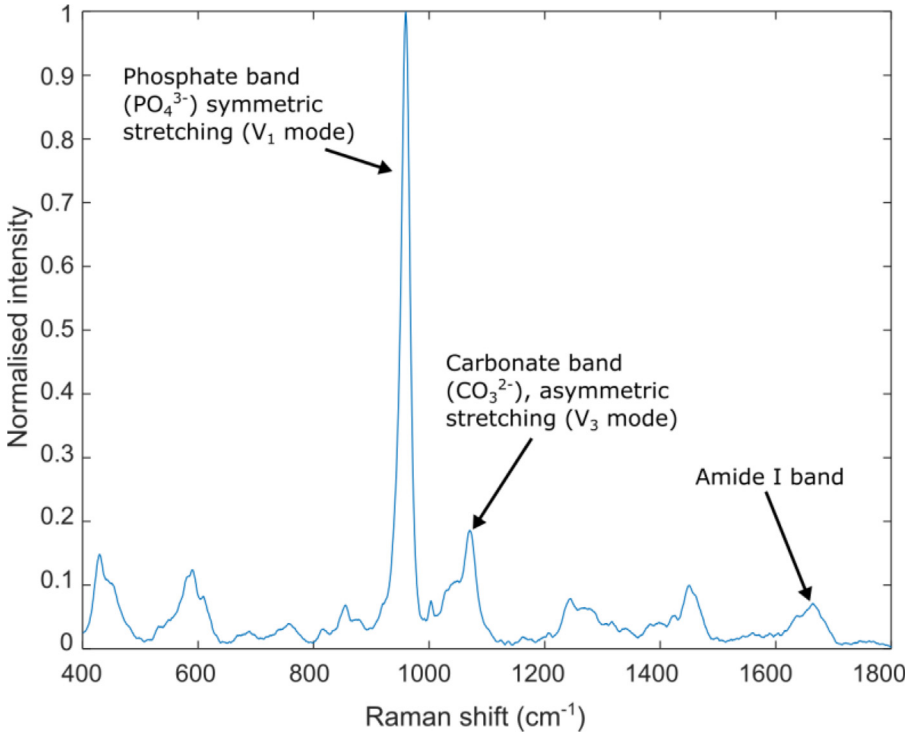

Fig. 2. Example of the obtained Raman spectra for the control sample. The most relevant bands are shown. Mineralisation is the amplitude ratio of the PO_4^{3-} to the amide I band, carbonate substitution is the ratio of the PO_4^{3-} to the CO_3^{2-} band and the crystallinity is the full-width at half-maximum (FWHM) of the PO_4^{3-} band.

with values reported previously for ovine [32] and human [49] bone. This guaranteed that the samples used in this research exhibited a proper chemical quality.

2.2. Drilling tests

Since drilling is highly used in orthopaedic surgeries (e.g. total knee arthroplasty, trauma interventions), it was chosen to study the damage induced to the sub-surface of the bone tissue by machining operations.

To avoid tissue degradation as much as possible, the drilling tests (Fig. 3) were conducted 6 h after the bone was acquired from a local butcher. After obtaining the $50 \times 40 \times 9$ mm^3 samples and prior to the drilling processes, the samples were kept at room temperature and immersed in saline solution. All samples were retrieved from a single mid-diaphysis bovine femur.

The drilling operations were performed with a typical surgical drill bit (i.e. 2 flutes, 4.5 mm diameter) [50] in the radial direction relative to the long axis of the bone (i.e. transverse direction relative to osteon orientation), as shown in Fig. 4. Twelve different drilling conditions were employed, with various spindle speeds (i.e. 600, 1200, 3000, 9000 RPM) and feed speeds (i.e. 30, 60, 120 mm/min), with no coolant whatsoever. Considering the intent of this research is to study the thermal damage, these cutting conditions were chosen to intentionally create both low and high temperature drilling scenarios in which the minimum temperature was higher than the necrosis threshold of 47 °C [39]. To verify this, a thermal camera (FLIR T460) was included in the experimental setup at ca. 500 mm away from the workpiece (Fig. 3) and pointing at the tool-bone interface at the drill entrance to measure the cutting temperatures. This provided a relative comparison of temperature rise for all the employed drilling conditions.

After drilling, the samples were immediately (i.e. within 20 min of drilling) cut into two sections along the hole axis (Fig. 4) and used for damage evaluation of the bone machined sub-surface. One half was used for histological analysis (i.e. necrosis evaluation) and the other one for micro-mechanical testing (i.e. changes in the micro-mechanical behaviour). However, to study the effects of high and low temperature drilling, only two of the twelve drilled samples were used for histology and micro-mechanics (Table 1).

The two selected cutting conditions produced the lowest (62 °C) and highest (110 °C) cutting temperatures, respectively, and therefore are expected to induce different levels of thermal damage to the bone. From here on, these two conditions are referred to as *low temperature, LT,* (cutting speed $V_c = 8.5$ m/min, feed rate $f_n = 0.2$ mm/rev, maximum temperature $T_{max} = 62$ °C) and *high temperature, HT,* (i.e. $V_c = 42.5$ m/min, $f_n = 0.01$ mm/rev, $T_{max} = 110$ °C), conditions, respectively.

2.3. Histology

Immediately (i.e. within 5 min) after sectioning the drilled samples, the histology samples were fixed for 48 h in 10% neutral formalin at room temperature to preserve the tissue and its cells (i.e. osteocytes) [19,51]. Afterwards, for decalcification, the samples were kept in a solution of 40 ml 65 vol% nitric acid, 20 ml 10 vol% formaldehyde and 340 ml deionised water for 10 days. The solution was changed for

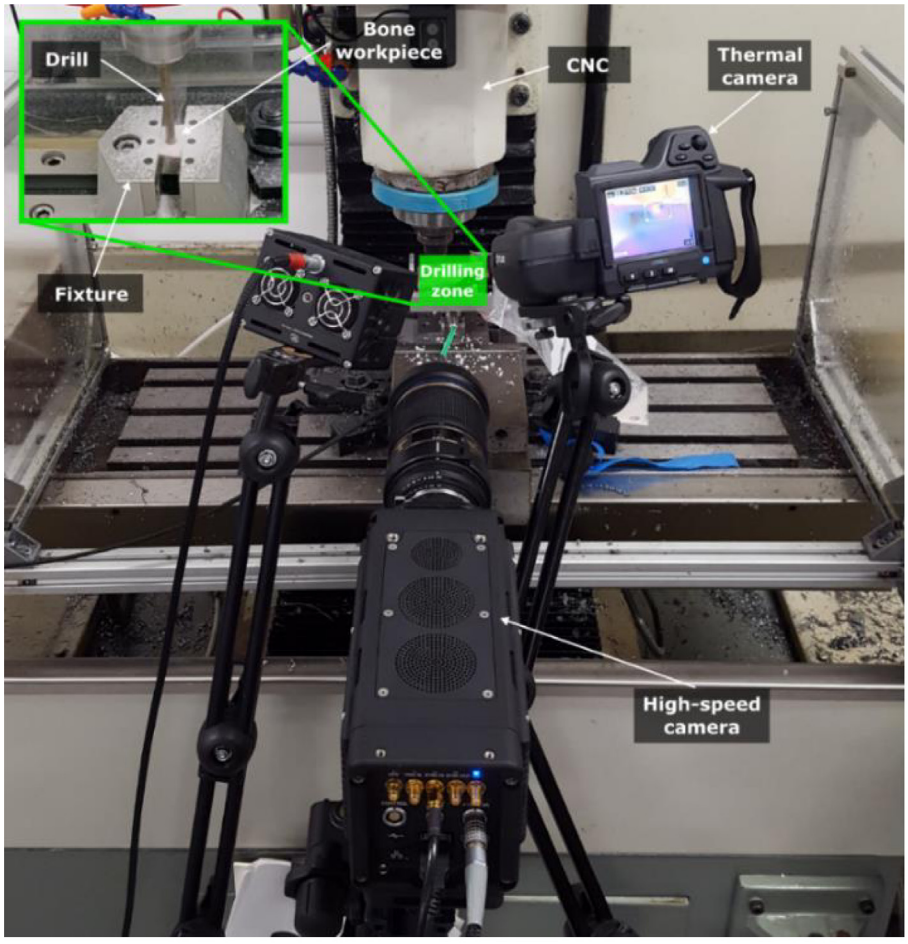

Fig. 3. Drilling trials setup. A CNC milling machine tool (1100 PCNC Tormach) was used for making the drilling experiments. A thermal camera (FLIR T460) and a high-speed camera (IDT Y4-S2 Motion Pro) were used during each drilling test to record the experiment data.

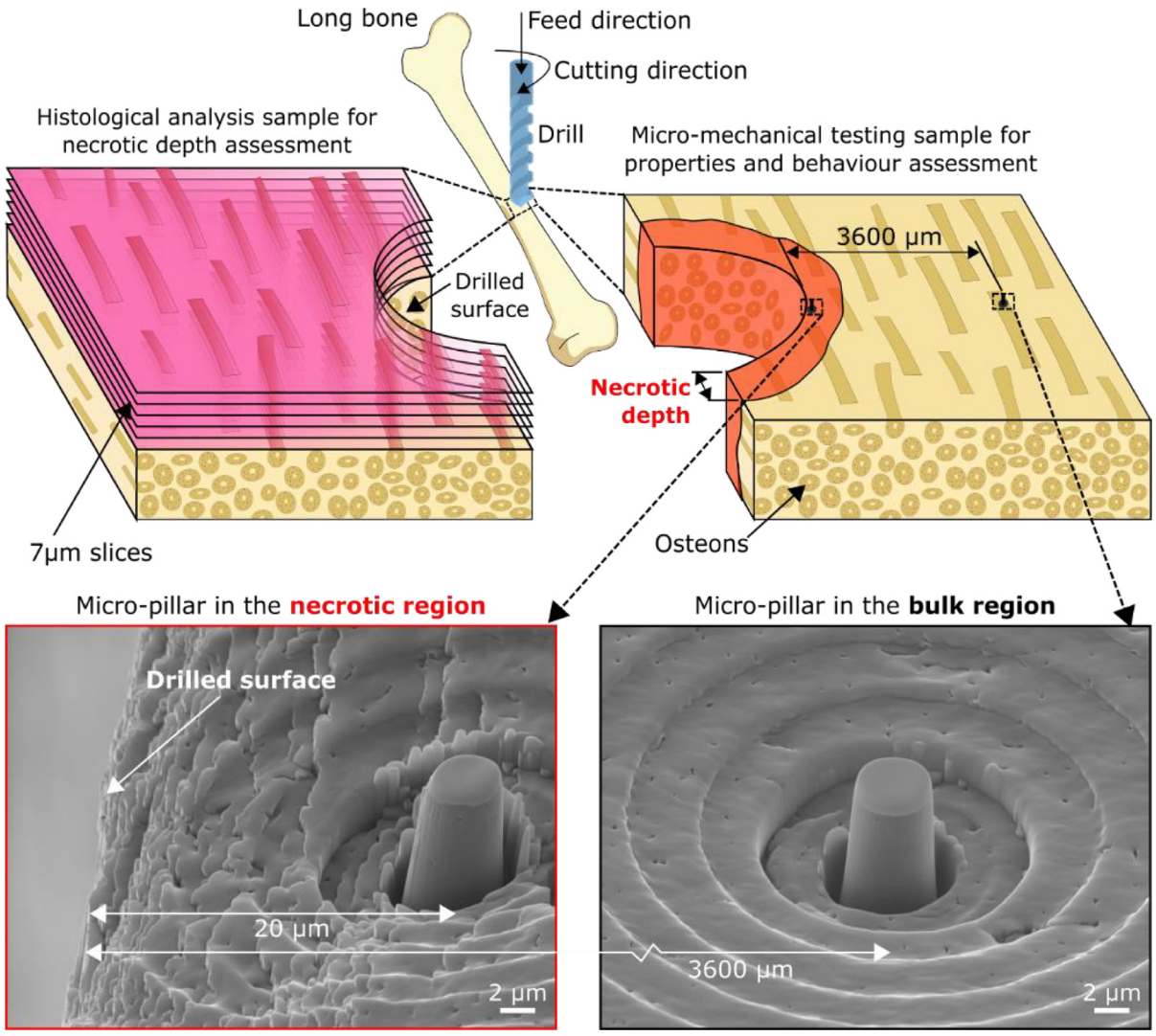

Fig. 4. Location of micro-pillars inside and outside the necrotic zone, and histological analysis of the drilled holes. After drilling, one half of the specimens (i.e. hole) was used for histological analysis (shown as pink slices) to evaluate the necrotic depth. The other half was used for fabricating micro-pillars with FIB inside the necrotic region (shown in red) and in the bulk material (shown in black) for evaluation of elastic and plastic properties, as well as to perform failure mode observations. (For interpretation of the references to colour in this figure legend, the reader is referred to the web version of this article.)

a fresh one each second day [21]. After this, the samples were dehydrated in a tissue processor (Leica TP 1020) by immersion in different alcohol baths with increasing alcohol percentage (i.e. 70%, 80%, 90%, 100%, 100%, 100%) for 1.5 h in each of the 70–90% alcohols and 1 h in each of the 100% alcohols. This was followed by two immersions in xylene for 1.5 h each and then finalised the dehydration process by immersion in two separate 2-h baths of paraffin to infiltrate into the porosities of the bone. Afterwards, each sample was mounted in paraffin, taking essential care of the drilling direction to leave the outermost cortical region of the sample in the cutting end of the paraffin-mounted section. Mounting was ensured by allowing at least 1 h of solidification in a cold environment. Paraffin-mounted samples were sectioned with a microtome (Leica RM2245) to obtain 7 µm thick slices that were stained with haematoxylin and eosin (H&E) to allow improved morphological observation of the tissue [51] under light microscopy. After staining, the samples were mounted in a mixture of distyrene, plasticiser and xylene (i.e. DPX) media and left to dry for at least 24 h prior to light-microscopy observation (Axioplan, Zeiss). Necrotic depth evaluation (i.e. measurement from the drilled surface to the disappeared osteocytes extent) were made in Fiji (ImageJ). Measurements were done manually for each image by measuring the radial distance from the drill site to the location with filled lacunae. At least 4 measurements were done for each slice and a total of 32 slices were used for the LT sample, while a total of 37 were used for the HT sample. A separate control sample (i.e. non-machined) was also used for histology to confirm that the sample

Table 1
Selected sample drilling conditions for histological and micro-mechanical analyses.

Drilling condition	Cutting speed, V_c (m/min)	Feed rate, f_n (mm/rev)	Coolant	Maximum measured temperature, T_{max} (°C)
Low temperature (LT)	8.5	0.20	None	62
High temperature (HT)	42.5	0.01	None	110

handling (i.e. polishing and manual grounding and cutting) did not induce necrosis to the tissue.

2.4. Micro-mechanics

To assess machining damage in terms of mechanical performance and properties, micro-testing (i.e. micro-pillar compression) was used as an approach for evaluating elastic and plastic properties inside and outside the necrotic (N) zone that was evaluated with the histological analysis.

The samples used for micro-mechanical testing were glued with silver adhesive (Agar Scientific) to SEM stubs and slightly polished (1 μm diamond particle suspension and 0.06 μm colloidal silica, employing fresh saline water rinsing with ultrasonic bath after each step) to remove any drilling debris to facilitate SEM imaging. Afterwards, the samples were air-dried for 12 h, subsequently being coated with a 25-nm gold layer via sputtering to minimise drift due to charging in SEM imaging.

Prior to micro-pillar FIB milling, a 1.25 μm platinum (Pt) protective layer was deposited on top of each pillar location. Afterwards, each micro-pillar was milled similarly to a previously established protocol [32] using a FEI Quanta200 3D FIB-SEM: circular trenches of 45 μm in diameter were milled at 7 nA to obtain 15 μm diameter posts; then, these were milled at 3 nA to obtain 7 μm diameter posts that were finally polished at 0.3 nA to obtain the final micro-pillar size of 5 μm in diameter and 10 μm long.

Micro-pillars were located in the bulk (B) material (i.e. 3600 μm radially away from the drilled surface) and in the necrotic (N) region (see Fig. 4) for both drilling conditions. In the LT sample 6 micro-pillars were fabricated (2 in the necrotic zone and 4 in the bulk zone); in the HT sample 9 micro-pillars were fabricated (4 in the necrotic zone, 3 in the bulk zone and 2 in between these zones). A total of 15 micro-pillars were successfully compressed.

Investigations on micro-pillar compression in brittle materials [52] have shown that pillars exceeding a threshold critical diameter, d_{crit}, are prone to crack development failures, whereas those with $d < d_{crit}$ tend to fail with ductile mechanism [53]. Furthermore, according literature [32], $d_{crit} > 5$ μm for ovine cortical bone in the radial direction. Therefore, all micro-pillars were fabricated with a nominal diameter of 5 μm and an aspect ratio of 2 [54]. In this manner, we assure that any failure mode transition (i.e. from ductile to brittle) that could be observed is a result of machining damage and is not related to micro-pillar size.

After fabrication, each pillar was inspected in a 7000 JEOL FEG-SEM at 50° specimen tilt and with different rotation angles for (i) a comprehensive pre-testing geometrical characterisation and (ii) to confirm the pillar was not located above a lacuna (Fig. 5). The micro-pillars were measured to be 4.94 ± 0.27 μm ($n = 15$) in diameter with an aspect ratio of 2.22 ± 0.21 μm (n = 15), making them of appropriate size for micro-pillar compression testing [54].

During inspection, it was detected that micro-pillars located at 20 to 50 μm away from the drilled surface (e.g. micro-pillar in the necrotic zone shown in Fig. 4) exhibited a rougher surface around them when compared to micro-pillars located in the bulk region due to the edge effect caused by FIB milling during the roughing pass. However, this edge effect does not adversely affect the use of these micro-pillars for compression testing since a finishing pass was also included in the FIB milling process that yielded a smooth micro-pillar surface. This was confirmed with several micro-pillars that behaved mechanically the same (i.e. both in stress-strain performance and failure mode) in the edge of the sample and in the bulk material (as shown in Fig. 9a).

All micro-pillars were compressed at a strain rate of $1.35 \times 10^{-3}\ s^{-1}$ until failure. This was done using a nanoindenter (Alemnis ASA, Switzerland) with a 6-μm flat diamond tip inside an SEM (FEI Quanta 650) under high vacuum conditions.

Load and displacement data were obtained for each pillar and were corrected for compliances associated with the platinum protective layer, nanoindenter frame and sink-in effect. The latter was performed following the Sneddon method [54] by assuming a 300 nm fillet radius [32]. Engineering stress-strain data was obtained following established protocols [30,32] and true stress-strain data was derived with the assumption of negligible volume change [55]. Data management was done both in AMMDA (Alemnis ASA, Switzerland) and Matlab. After compression, the micro-pillars were inspected in a 7000 JEOL FEG-SEM for failure mode identification with a 50° specimen tilt.

3. Results

3.1. Macro-damage on the machined bone surface

As initial investigatory step (i.e. before histology and micro-mechanical analyses), a separate set of the LT and HT drilled samples were inspected for macro-damage by using SEM in a low vacuum (LV) environment. Initially, it seemed that the HT condition exhibited a smooth "crack-free" surface (Fig. 6a), while the LT condition sample presented large cracks on the machined surface (Fig. 6c). Such an effect is unexpected as the latter drilling condition presented a lower temperature (i.e. 62 °C) and as such, should not present a large extend of surface damage.

To verify if the operating vacuum conditions of SEM might have played a contribution to crack propagation of the bone's composite structure, the samples (after three days of air-drying) were coated with gold and inspected again under SEM in a high vacuum (HV) environment. The LT sample (Fig. 6d), showed no signs of crack growth. Contrary to this, the HT sample, which previously presented "crack-free" and smooth surface, now revealed the appearance of some minor cracks (Fig. 6b). This implies that some of the machined surface of the bone was smeared due to the high cutting speed and slow feed rate, creating a 'deceiving' smooth appearance with minor cracks laying underneath.

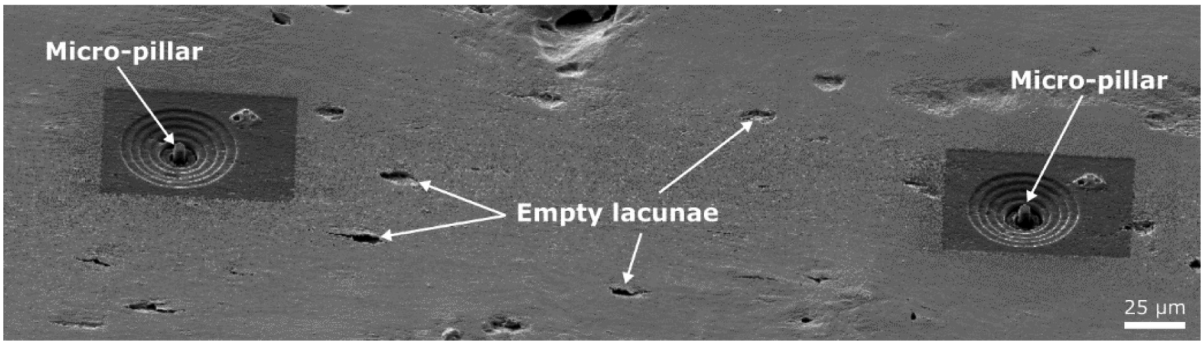

Fig. 5. Example of a cluster of two micro-pillars in the high temperature drilling conditions sample. The empty lacunae are easily visible since they normally are within 5–20 μm long [15], which makes them comparably larger to the nominal diameter of the micro-pillars (i.e. 5 μm).

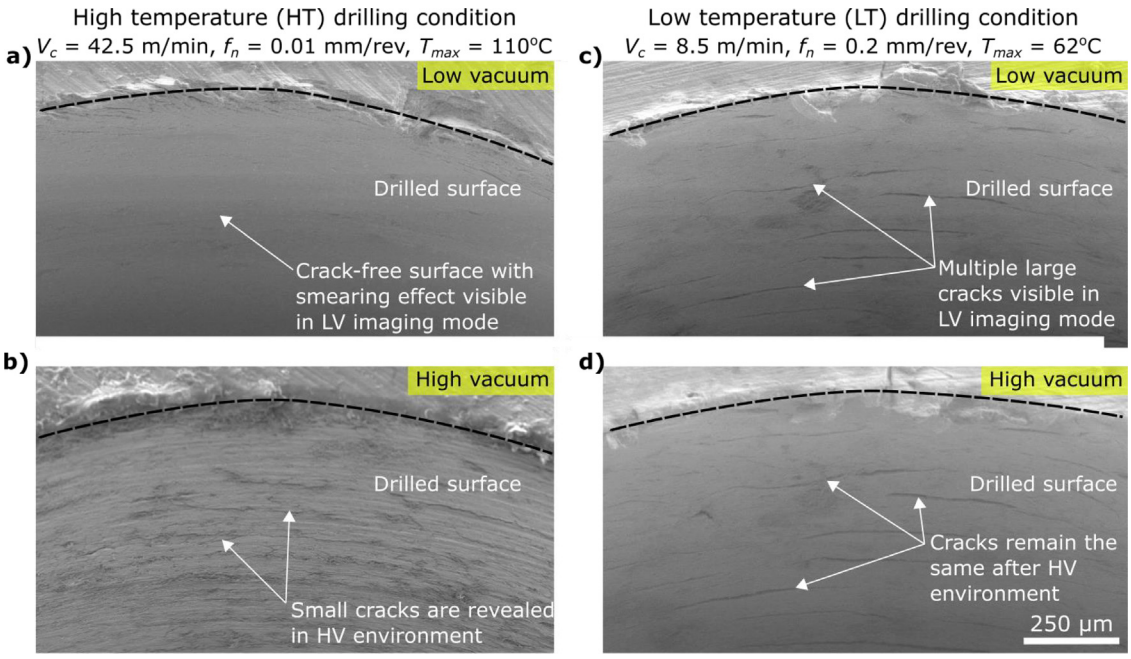

Fig. 6. Macro-level effect of drilling conditions upon crack formation and surface smearing when using high (HT) and low (LT) temperature drilling conditions in low and high vacuum SEM. (a,b) *As-machined bone surface with HT conditions yielding intense thermal fields (T_{max} = 110 °C):* (a) LV imaging immediately performed after drilling revealed a deceiving "crack-free" surface with a smearing effect, giving it a smooth appearance; (b) HV imaging carried out after 72 h of air-drying revealed minor cracks that were not visible in LV SEM. (c,d) *As-machined bone surface with LT conditions yielding lower level of thermal fields (T_{max} = 62 °C):* (c) LV imaging immediately performed after drilling revealed a surface with large cracks; (d) HV imaging carried out after 72 h of air-drying revealed no further crack growth.

The smearing effect was not seen following low temperature drilling conditions, with damage appearing immediately after the cutting operation in the form of large cracks. At first instance, this was not expected as it is envisioned that a high temperature drilling condition will generate more cracks than a lower-temperature one. However, two points need to be addressed: (i) The LT drilling condition is adopted to minimise the cutting temperature, and hence to minimise the necrotic depth, but this does not inherently result in a better surface quality after drilling. (ii) The lack of cracks in the HT sample can be explained with the cutting mechanics of bone. Cortical bone exhibits different chip formation mechanisms [10], one of which is fracture mode at the largest chip thicknesses, which results in a cracked surface. Another is shearing mode at the lowest chip thicknesses, resulting in a smooth surface. Since the HT condition has a considerably lower (20 times) feed rate than the LT condition, it results in lower thrust forces with a smoother chip type and an uncracked surface. However, even though the HT condition induces less macro-cracks to the tissue, it is the one that affects the most in terms of necrosis and micro-mechanical properties, as it will be shown further.

This macro-level analysis reveals that the cutting process has a considerable effect on the bone surface and temperature, depending on the cutting conditions. Furthermore, the hierarchical and biological nature of the bone raises questions about the effects of such behaviour to the micro-mechanical properties of the tissue, as well as the repercussions to the living cells near the drilled surface. Therefore, the understanding of the micro-mechanical behaviour in the machined sub-surface and the necrotic depth into the bone by means of micro-mechanical testing and histological analysis can reveal an integrated and comprehensive damage evaluation.

3.2. Necrotic damage in the machined bone sub-surface

Thermal necrosis is induced to the tissue depending on both the maximum temperature and the amount of time that said temperature is held within the tissue. Temperatures as low as 47 °C and 50 °C are enough to cause necrosis if maintained for periods of 60 and 30 s [39], respectively. After drilling, a portion of each sample was analysed by histological means (see Fig. 4) to understand the relationship of necrotic depth to cutting conditions (e.g. temperature), by measuring the semi-annular thickness of the zone with dead osteocytes (empty lacunae).

We confirmed that greater temperatures produce larger necrotic zones (see Table 2), since the LT condition (T_{max} = 62 °C) created a necrotic depth of 49 ± 3.9 µm (n = 162) (Fig. 7a & b), while the HT condition (T_{max} = 110 °C), possessing a more intense thermal field, yielded a necrosis penetration zone of 419 ± 33.2 (n = 185) (Fig. 7c & d). Under both sets of conditions, the necrotic zone locally hinders the bone healing capacity due to the lack of osteocyte activity; this makes the recovery more difficult for implant bonding and localised healing [56,57]. Nevertheless, the healing capabilities of necrotic tissue are not within the scope of this research.

To confirm that sample handling and preparation (i.e. polishing, manual grounding and cutting) did not induce a necrotic effect to the bone, a control sample was analysed as well (Fig. 7e & f). The histological analysis showed no signs of necrosis whatsoever, as all lacunae appeared filled, effectively proving that the followed protocol is acceptable and does not induce any necrotic damage to the tissue. Hence, the previously mentioned necrotic depths for the LT and HT conditions were induced only by the drilling operation.

The micro-mechanical response of the necrotic zone could reveal micro-level behaviour changes under different loading conditions. As this response has not yet been addressed in the literature, micro-mechanical testing was performed inside and outside the necrotic region in both drilled samples.

It is also interesting to observe that the Raman spectra before and after drilling (in the drill site) remains unchanged since the high temperatures achieved during the drilling experiments (max. 110 °C) are unable to create significant chemical changes in the bone that could be measured with this technique, as shown in Fig. 8. This is consistent with other studies where thermal damage assessment with Raman spectroscopy is difficultly employed when bones are burned at temperatures lower than 700 °C [58].

Table 2
Necrotic depth measurements, as obtained with histological analysis.

Drilling condition	Maximum measured temperature, T_{max} (°C)	Necrotic depth (μm), avg ± std dev	Number of measurements, n
Low temperature (LT)	62	49 ± 3.9	162
High temperature (HT)	110	419 ± 33.2	185

3.3. Micro-mechanics of the machined bone sub-surface

To assess the micro-mechanical behaviour of bone near the drilled surface, micro-pillar compression tests have been performed in the sub-surface at different radial distances in two distinct regions: (i) on the bulk (B) material, where no damage is expected (3600 μm beneath the drilled surface) and (ii) on a region near the machined sub-surface (within the necrotic (N) zone and near the drilled surface). Refer to Fig. 4 for visual representation of the locations.

3.3.1. Micro-pillars in the low temperature (LT) drilling condition sample

The micro-pillars in both the bulk (Fig. 9a - B_{LT}, sky colour) and necrotic (Fig. 9a - N_{LT}, black colour) regions of the LT drilling condition behaved similarly in terms of stress-strain. These pillars displayed an elastic modulus of 15.78 ± 1.56 GPa ($n = 6$), yield strength of 0.34 ± 0.02 GPa (n = 6) and ultimate strength of 0.67 ± 0.04 GPa (n = 6), in fair agreement with previously published results of micro-pillars in damage-free cortical bone in the transverse direction [32]. Besides displaying such an unaffected micro-mechanical behaviour, the post-yield mechanism until failure was exclusively governed by slipping along a single shear plane (Fig. 9b), clearly showing the characteristic shearing failure mode of undamaged cortical bone in the micro-scale [32]. These results indicate, for the first time, that low temperature ($T_{max} = 62$ °C) machining produces no changes in the micro-mechanical behaviour, implying that micro-mechanical damage is inexistent in both the necrotic (N_{LT}) and bulk (B_{LT}) regions of the machined sub-surface.

3.3.2. Micro-pillars in the high temperature (HT) drilling condition sample

The micro-pillars in the bulk material (Fig. 10a - B_{HT}, blue colour) of the HT sample revealed a congruent stress-strain behaviour (i.e. within standard deviation) as those from the LT drilling sample, with elastic modulus of 16.01 ± 0.72 GPa ($n = 3$), yield strength of 0.36 ± 0.04 GPa (n = 3) and ultimate strength of 0.65 ± 0.01 GPa (n = 3). Furthermore, these micro-pillars (B_{HT}) also failed by shearing (Fig. 10b), as those from the LT drilling conditions (Fig. 9b); in both cases, the failure mode is clearly identifiable and in agreement with another bone micro-pillar compression study [32]. This behaviour confirms that in high temperature drilling ($T_{max} = 110$ °C), the micro-mechanical behaviour of bone is not affected at large distances (i.e. 3600 μm) from the drilled surface (away from the necrotic layer).

Micro-mechanical damage was detected for micro-pillars closer to the drilled surface in the HT sample in the form of reduction of properties. The pillars within the necrotic layer (Fig. 10a - N_{HT}, green colour) exhibited an elastic modulus 42% lower (9.20 ± 1.54 GPa, $n = 4$) than the unaffected bone. Ultimate strength was also lower by 41% (0.39 ± 0.02 GPa, n = 4). Nonetheless, the yield strength was less affected, with only a 15% reduction (0.29 ± 0.03 GPa, n = 4). All the pillars confined to this region (N_{HT}) failed by splitting of axial cracks (Fig. 10e) which corresponds to a brittle failure mode.

This behaviour shows that if high temperatures occur during drilling, the damaged zone is not only constrained to a greater cellular death extent, as histological analysis suggests (Fig. 7 and Table 2), but also to a considerably different micro-mechanical post-yield behaviour with smaller elastic and plastic regions.

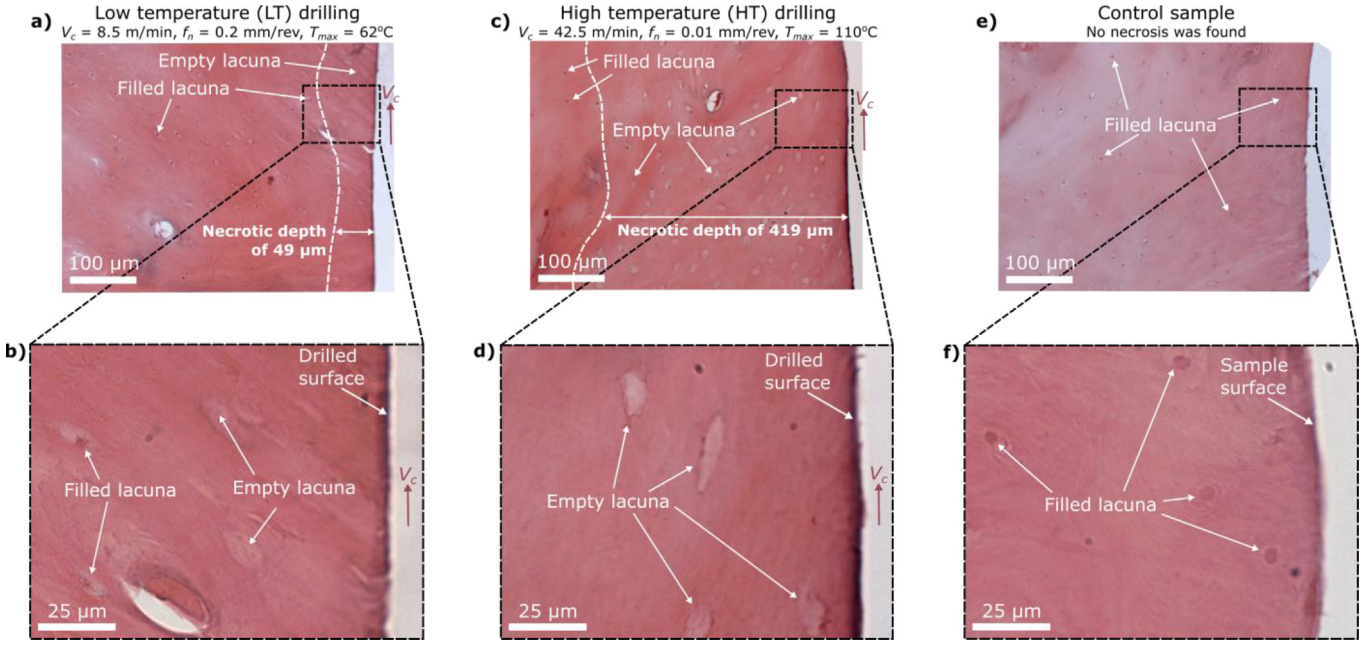

Fig. 7. Evaluation of the necrotic depth by histological analysis on the bone surface after using low (LT) and high (HT) temperature drilling conditions. (a,b) *At LT conditions:* (a) At low magnification, most lacunae seem to be filled with osteocytes both near and far from the surface; (b) Higher magnification reveals that empty lacunae are confined to a necrotic distance of 49 ± 3.9 μm ($n = 162$). (c,d) *At HT conditions:* (c) Even at low magnification it is evident that the greater cutting temperature induced an 8-times larger necrotic depth of 419 ± 33.2 μm ($n = 185$) in average; (d) Higher magnification shows that all osteocytes near the drilled surface disappeared during drilling due to the high temperatures achieved in the sub-surface. (e,f) The control sample showed no signs of necrosis, as all lacunae are filled, both near and far from the surface.

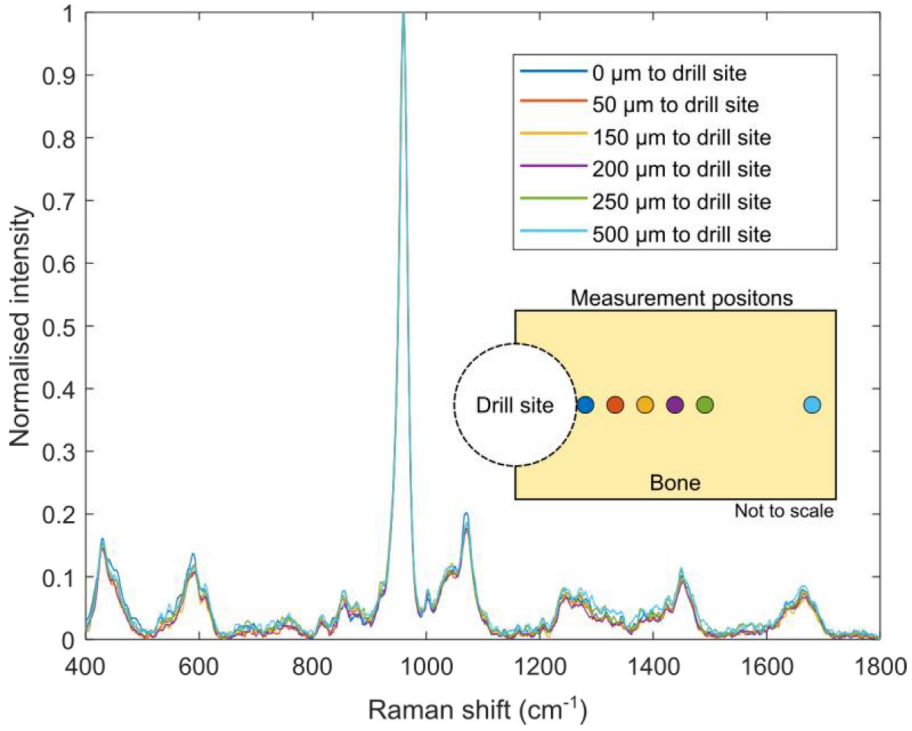

Fig. 8. Raman spectra near the drill site after high temperature drilling (T_{max} = 110 °C). Raman spectroscopy was employed to quantify the thermal damage in the HT sample. However, for positions both near (within the necrotic region) and far (outside the necrotic region) from the drill site, the spectrum remains unchanged and in congruence with that of Fig. 2. For all points, the crystallinity, mineralisation and carbonate substitution are consistent (i.e. within standard deviation) with that of the control sample (Fig. 2).

To assess the existence of a transition zone between the necrotic (N_{HT}) and the undamaged (B_{HT}) regions of the HT sample, additional micro-pillars were fabricated on intermediate (I) regions (i.e. I_1 and I_2) outside of the necrotic area (refer to Fig. 11 and the legend of Fig. 10). These intermediate locations for pillars I_1 and I_2 were set to 2700 and 1500 µm from the drilled surface, respectively. The analysis revealed that the pillar closer to the bulk material (Fig. 10a – I_1, yellow colour) behaved similarly to the pillars in the bulk region (Fig. 10a – B_{HT}, blue colour), with elastic modulus and yield stress within the standard deviation of the pristine values (15.17 GPa and 0.35 GPa, respectively); and just the ultimate stress lower by 20% (0.53 GPa).

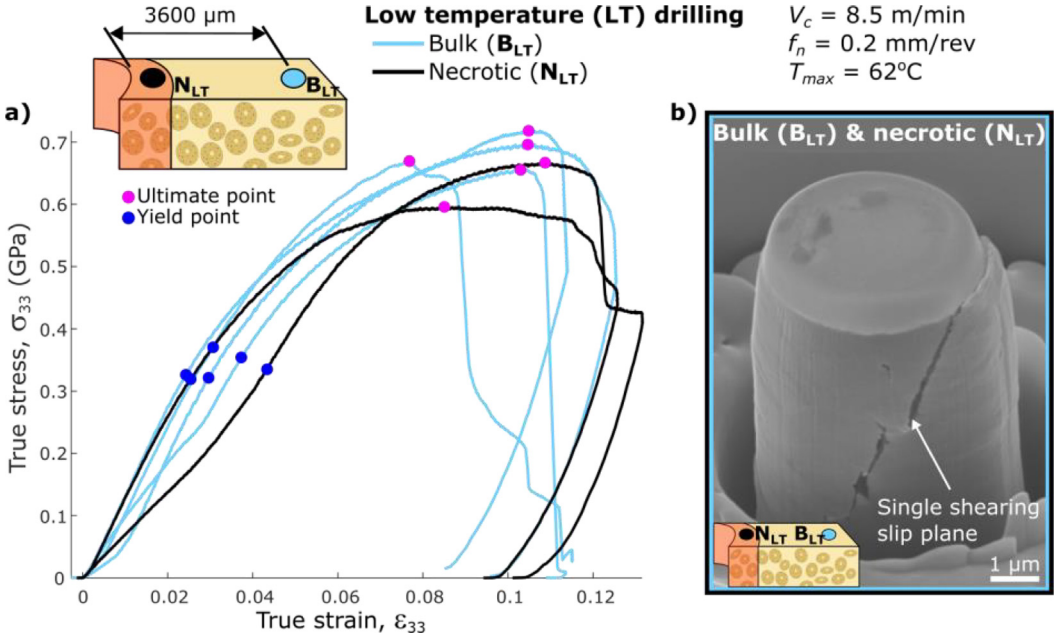

Fig. 9. Stress-strain curves and failure micrograph of micro-pillars from the low temperature (LT) drilling condition in the necrotic (N_{LT}) and bulk (B_{LT}) regions. (a,b) *Micro-pillars in the bulk and necrotic zones of the LT drilling condition exhibited the classic behaviour of undamaged cortical bone.* (a) Stress-strain curves showing no difference between mechanical performance in the bulk (B_{LT}) and necrotic zones (N_{LT}) obtained in LT drilling conditions. (b) Representative micro-pillar of both the bulk (B_{LT}) and necrotic (N_{LT}) zones, which failed exclusively by slipping along a single shear plane.

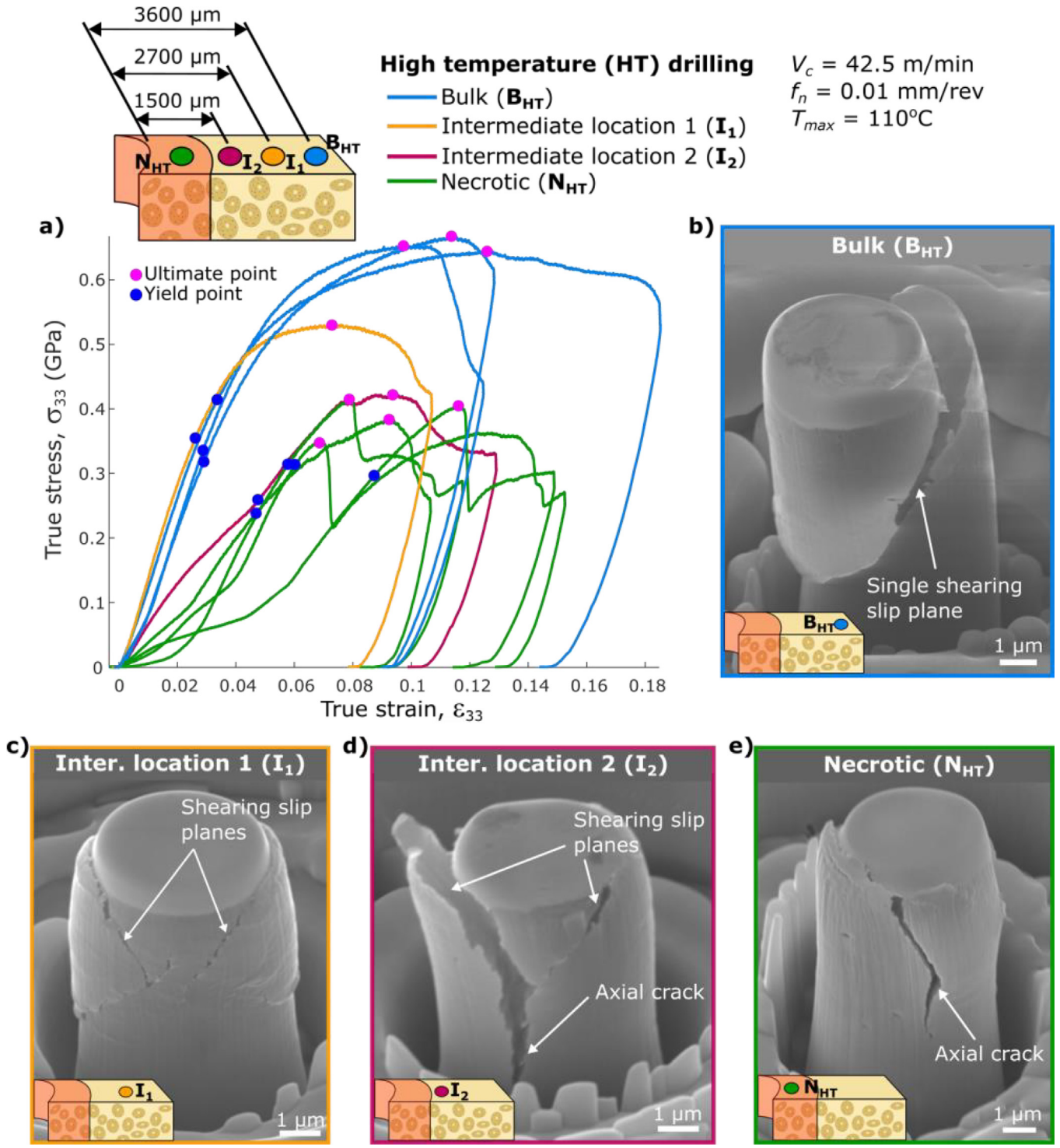

Fig. 10. Stress-strain curves and failure micrographs of micro-pillars from the high temperature (HT) drilling condition in the necrotic (N_{HT}), intermediate (I) and bulk (B_{HT}) regions. *Micro-pillars from the HT sample exhibited different behaviours depending on their location.* (a) Stress-strain curves, showing that bulk micro-pillars (B_{HT}) behaved as undamaged bone (i.e. similar to Fig. 9a) and that the performance decreases as the micro-pillar location gets closer to the drilled surface. (b) Micro-pillars located in the bulk region (B_{HT}, blue colour) failed by slipping along a single shear plane. (c) The micro-pillars located in intermediate location 1 (I_1, yellow colour) exhibited a two-plane shearing failure mechanism. (d,e) Micro-pillars located in intermediate location 2 (I_2, magenta colour) and necrotic (N_A, green colour) zones failed by axial splitting. (For interpretation of the references to colour in this figure legend, the reader is referred to the web version of this article.)

Nonetheless, the pillar closer to the necrotic region (Fig. 10a – I_2, magenta colour) behaved similarly (i.e. within standard deviation) to the pillars inside the necrotic layer (Fig. 10a – N_{HT}, green colour), exhibiting an elastic modulus, yield stress and ultimate stress of 8.86 GPa, 0.26 GPa and 0.41 GPa. These results confirm that the mechanical properties of the bone degrade in a gradual manner from the pristine behaviour in the bulk (B_{HT}) material to a weakened performance in the necrotic (N_{HT}) layer. This phenomenon only occurs if high temperatures occur during the cutting operation, such as with HT conditions (Table 1).

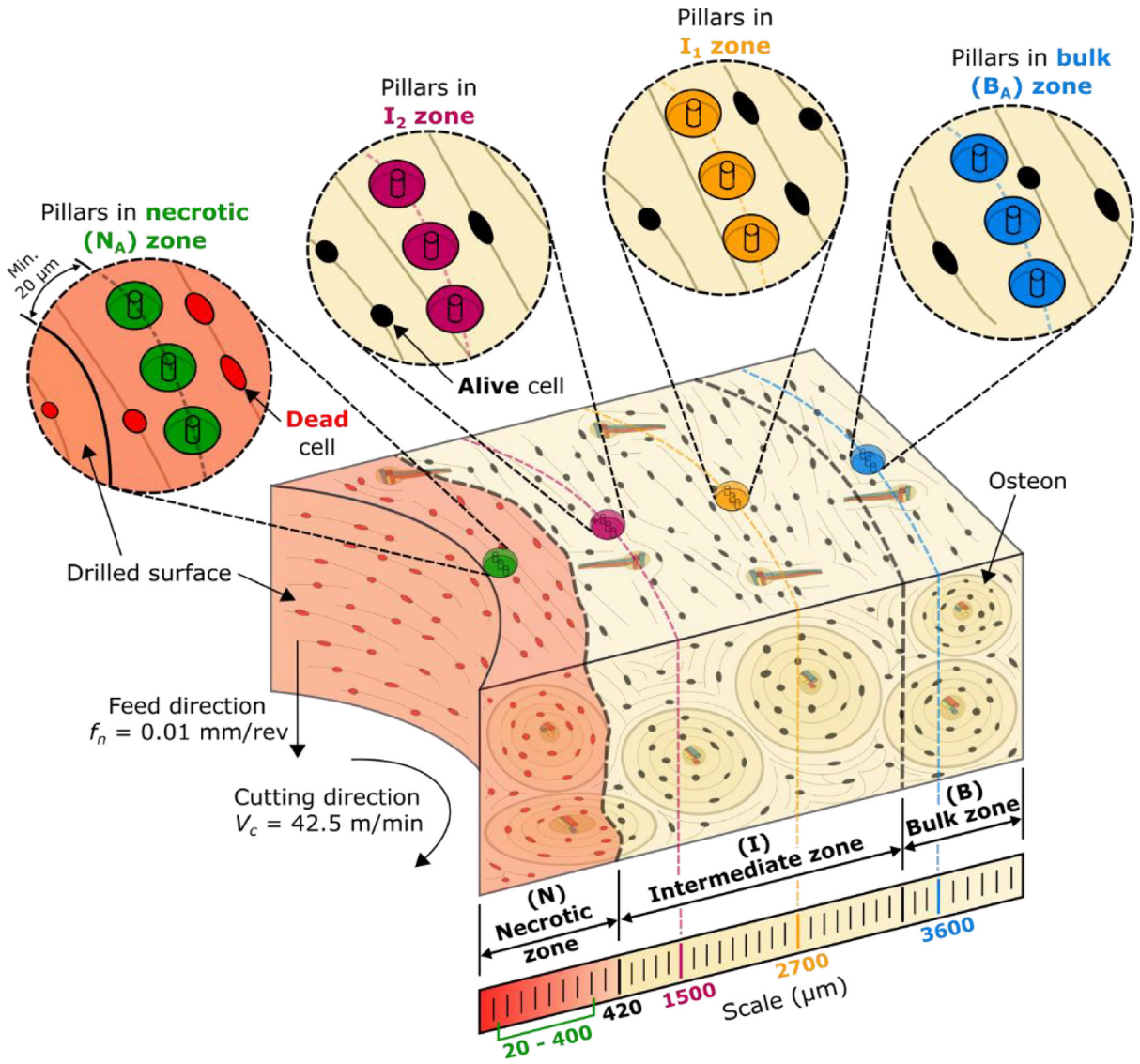

Fig. 11. Schematic of the micro-pillar cluster locations in the high temperature (HT) drilling conditions sample. The micro-pillars in the necrotic zone (N_{HT}, green colour) are located within 20 to 400 µm away from the drilled surface, since the necrotic (N) depth in this condition is 419 ± 33.2 µm ($n = 185$) (Fig. 7c & d). Micro-pillars in the bulk material (B_{HT}, blue colour) are located at 3600 µm from the drilled surface. To assess if there is a transition of the micro-mechanical behaviour between the necrotic (N_{HT}, green colour) and bulk (B_{HT}, blue colour) zones, additional pillars were fabricated in two intermediate locations (i.e. I_1 and I_2, shown in yellow and magenta colours, respectively). (For interpretation of the references to colour in this figure legend, the reader is referred to the web version of this article.)

Failure mode analysis of the micro-pillars in the transition layer showed that pillars in intermediate location 1 (I_1, yellow colour) failed by the development of two slip planes with localised shear (Fig. 10c), while the pillars in intermediate location 2 (I_2, magenta colour) failed by axial splitting (Fig. 10d). This proves that the mechanical properties are gradually transitioning from the undamaged (B_{HT}) region to the necrotic (N_{HT}) zone, and so does the failure mode. The failure mode shifts from single-plane shearing (bulk region, B_{HT}) to two-plane shearing (intermediate region) and then to axial splitting in the necrotic (N_{HT}) region, indicating a ductile-to-brittle transition going from the undamaged bulk (B_{HT}) region to the necrotic (N_{HT}) zone.

According to classic fracture mechanics [59], cracks can propagate in one of three main modes ((I) opening; (II) in-plane shearing; (III) out-of-plane shearing), depending on the direction of loading. The observed brittle failure (axial splitting, Fig. 10d & e) corresponds to a mode I fracture, consisting of the axial crack that propagates from the intersection point of two slip planes, as shown in Fig. 10d. This type of fracture can be modelled at the nano- and micro-scales employing dislocation-based models [60]. The micro-pillar fracture toughness, G_c, for this case can be calculated as [36]:

$$G_c = \frac{1}{16E}\pi\sigma_{ult}^2 d \sin\phi \cos^3\phi \quad (1)$$

where E is the elastic modulus, φ is the shear plane angle, σ_{ult} the ultimate stress and d the pillar diameter. Calculations for each pillar yielded an average toughness of 6.68 ± 1.14 J/m^2 ($n = 9$) for the pillars that failed with ductile mechanism (Figs. 8b & 9b, & Supplementary Movie S1) and 4.24 ± 1.03 J/m^2 ($n = 5$) for the pillars that failed with axial splitting (Fig. 10d & e, & Supplementary Movie S2). These results indicate that pillars in the necrotic zone of high temperature drilling have a mode I fracture toughness that is 37% lower than that from pillars in the damage-free bone, implying that they require less energy to fail by splitting and are more susceptible to behave in a brittle manner. Such reduction in toughness, as well as the weaker elastic performance, makes the machined sub-surface more prone to this type of fracture under a brittle regime if subjected to stress.

4. Discussion

During bone cutting, besides the possibility of inducing cracks at the macro-scale, the cells within the tissue are also exposed to damage (i.e. necrosis) by the thermal loads applied during the machining process. To assess this type of damage (i.e. cellular death), histology has been used as the gold standard for many years, and therefore it was employed in this work to assess the necrotic depth for both cutting conditions studied, clearly revealing that a higher temperature (i.e. 110 °C) results in a deeper necrotic layer (419 ± 33.2 μm, n = 185) when compared to a lower temperature drilling (i.e. 62 °C) with less necrosis (49 ± 3.9 μm, $n = 162$).

From an engineering standpoint, bone could be regarded as a structural component of the human body, as it sustains mechanical loads. Therefore, not only its biological assessment (i.e. necrosis evaluation) is of relevance, but also its mechanical performance. With the intention of studying the material behaviour at the micro-level after been exposed to large temperature via a machining process, micro-mechanical testing (i.e. micro-pillar compression) was performed inside (near the machined surface) and outside (in the bulk region) the necrotic region.

The micro-mechanical tests showed no changes nor in properties (i.e. exhibited pristine properties) nor in failure mode (e.g. exhibited ductile failure with shearing mechanism) for pillars located in the low temperature (LT) sample, both inside the necrotic (N_{LT}) region and in the bulk (B_{LT}) zone. This was also the case for the micro-pillars in the high temperature (HT) sample located in the bulk (B_{HT}) region. Nevertheless, reduction in properties was quite significant for micro-pillars located in the necrotic (N_{HT}) region of the high temperature (HT) sample, displaying an elastic modulus, ultimate strength and yield strength reduced by −42%, −41% and − 15%, when compared to the undamaged pillars. Furthermore, these set of pillars (N_{HT}) displayed a dominant brittle failure characterised by a mode I fracture (i.e. axial crack, Fig. 10d & e).

The observed failure mode shift (from ductile to brittle) raises questions of the nature that drives such a drastic change in the microstructure to behave this way after exposure to high cutting temperatures (i.e. 110 °C). One or more phenomena could be occurring in the bony structure that makes it shift this way, such as a local dehydration effect surrounding the drill site.

Bone naturally possesses water at all its hierarchical levels, including pore-level water in the microstructure (i.e. within the Haversian canals, Volkmann's canals and the lacuno-canalicular system), loosely bound water in its ultrastructure and nanostructure (i.e. within the lamellae, the collagen chains and the mineral crystals), and tightly bound water at the molecular scale and at the structural level (i.e. in the apatite structure) [61]. Prior to the drilling experiments, the samples were kept at room temperature and immersed in saline solution; hence, it is expected that they retained a significant amount of water up to when the drilling started. During the high temperature drilling process, the measured temperature reached a maximum of 110 °C, which by itself is above the boiling temperature of water at atmospheric pressure. Therefore, it could be intuitively thought that bone regions near the drill site, which were exposed to the highest temperature build-up, lost some of their water content due to the exposure to such a high temperature; hence, creating a local dehydration effect. Furthermore, it is well known that dehydration increases the brittle behaviour in bone [61–63] both in compressive and tensile loading, which could explain the observed micro-pillar failure mode shift from ductile to brittle shown in Fig. 10. However, the literature also points out that as the brittle behaviour increases with dehydration, the stiffness and strength of the bone should also increase, which is opposite in this case: with high temperature drilling the brittle behaviour increased, but the stiffness and strength decreased. This does not inherently imply that local dehydration is not the explanation behind these results, but that it could be occurring in parallel with other phenomena.

Some explanations for the decremental properties in the locally dehydrated region are, for example, thermally induced residual stresses that are able to leave the material in a pre-loaded state, or changes to the nanostructure and molecular structure related to temperature but not to water. Nevertheless, these are other fields of study by themselves and out of the scope of this research. Whether any of them are occurring or not, more in-depth research is required to properly address them, as they are only plausible explanations of the underlying phenomena behind the presented results of micro-pillar compression testing for assessing machining-induced thermal damage in cortical bone.

In addition, cortical bone is a porous structure [3], meaning that the localised porosity in each micro-pillar may vary. Therefore, some serrated trends in the stress-strain curves may be observed (see Fig. 10a - N_{HT}, green colour) due to the collapse and densification process that occurs when a local porosity is collapsed during compression of the micro-pillar. In the future, it will be valuable to include local porosity assessments to improve the understanding of the stress-strain behaviour of bone under uniaxial compression micro-testing.

Usually, following the bone cutting process in a surgical environment, an implant is placed in intimate contact with the machined surface and, to prevent early stage failures of the implant, bone overheating must be avoided [64]. The main reason for this precaution is based on histological analysis, since at greater temperatures the osseointegration process is hindered with necrosis. Nevertheless, here we have shown that once high temperatures do occur, not only the necrotic layer is deeper, but an even greater heat-affected transition zone extends beyond the necrotic region. This implies that a larger volume of the bone is negatively affected from the mechanical perspective than from the biological standpoint, i.e. more volume of affected bone surrounding the implant when considering altered mechanical properties than when considering the quantity of dead cells. The hindered osteocyte activity in parallel with the lower mechanical strength could significantly alter the remodelling process of bone, since it has been proven that the remodelling process is not only sensible to necrosis, but also to the induced loads in the tissue [65]. Nevertheless, the results shown here are limited to ex-vivo bone in a non-clinical environment, and so further research would be required to study the bone micro-mechanical surface integrity and its impact on implant applications and the bone healing process.

With this research, an important aspect that has not been reported before comes to light: thermal damage manifests not only as necrosis in a bone machining operation, but also as micro-mechanical properties reduction and increased brittle behaviour near the machined sub-surface. In our studied case, when high temperatures (110 °C) occur during bone cutting, a weak micro-mechanical layer in the machined sub-surface is generated. This layer is larger than the necrotic region and exhibits a brittle behaviour with lower modulus (−42%), ultimate strength (−41%) and yield strength (−15%) than healthy undamaged bone. We have successfully proven this for high temperature drilling condition, where the micro-pillars in this region failed by axial splitting due to their reduction (−37%) in toughness for this type of fracture. These findings unveil new knowledge about the complex material behaviour of bone from an engineering perspective.

5. Conclusion

An experimental study was carried out to assess the machining-induced thermal damage in cortical bone after drilling with low (LT) and high (HT) temperature drilling conditions, which produced mild ($T_{max} = 62$ °C) and intense thermal fields ($T_{max} = 110$ °C), respectively, during the machining operation. SEM analysis showed that the gross appearance of the machined surface could be deceiving, as LT drilling produced evidently large cracks, while HT drilling produced a smearing effect that might appear smooth, but in fact has minor cracks lying underneath. Histological analysis and in-situ micro-pillar compression tests revealed that high temperature drilling produces an 8-times larger

necrotic depth (419 ± 33.2 μm, $n = 185$), when compared to low temperature drilling (49 ± 3.9 μm, $n = 162$); clearly showing that the higher the temperature, the larger the necrotic damage. Furthermore, in high temperature drilling, the micro-pillar failure mode analysis revealed that the microstructure shifts from being ductile in the bulk, to brittle and mechanically weaker (up to −42% reduction in elastic modulus, −41% in ultimate compressive strength and − 15% in yield strength) near the machined surface. It was found that this brittle layer can extend to at least 1500 μm away from the machined surface, which is more than 3 times the necrotic depth. This brittle layer was found to be inexistent in low temperature drilling, where micro-pillars in the necrotic layer retained both their pristine properties and their ductile failure mode.

This study reveals that the traditional histological analysis, which is valuable for assessing the amount of cellular death, could be complemented with micro-mechanical analysis to yield a full bone damage evaluation that accounts for both biological and mechanical assessments. Furthermore, the method here presented should be extrapolated to assess in-vivo or in-vitro bone after a surgical intervention where temperature build-up could occur in the bone-tool interface (such as in drilling, burring, milling, grinding or sawing associated with orthopaedics, dentistry, maxillo-facial surgery or neurosurgery) to study the micro-mechanical integrity of the tissue both as machined and as it heals post-surgery.

Supplementary data to this article can be found online at https://doi.org/10.1016/j.matdes.2020.109215.

Data and materials availability

All data needed to evaluate the conclusions in the paper are present in the paper. Additional data related to this paper may be requested from the authors.

CRediT author statement

Jose A. Robles-Linares: Conceptualization, Methodology, Validation, Formal analysis, Investigation, Data curation, Writing - Original Draft, Writing - Review & Editing, Visualization. **Dragos Axinte**: Conceptualization, Methodology, Visualization, Supervision, Funding acquisition, Writing – Review and Editing, Project administration. **Zhirong Liao**: Conceptualization, Methodology, Supervision, Writing – Review and Editing. Andres Gameros: Conceptualization, Methodology, Supervision, Writing – Review and Editing.

Declaration of Competing Interest

The authors declare that they have no known competing financial interests or personal relationships that could have appeared to influence the work reported in this paper.

Acknowledgments

We thank Mr. I. Ward and Ms. D. McLean from the School of Life Sciences, University of Nottingham, and Dr. C. Parmenter from the Nanoscale and Microscale Research Centre (nmRC), University of Nottingham, for their support. This work was supported by The University of Nottingham, the Mexican National Council for Science and Technology (CONACYT), the Nottingham Research Fellowship programme and the National Natural Science Foundation of China (No. 51975302).

References

[1] J. Heřt, P. Fiala, M. Petrtýl, Osteon orientation of the diaphysis of the long bones in man, Bone. 15 (1994) 269–277, https://doi.org/10.1016/8756-3282(94)90288-7.
[2] J.D. Currey, Bones: Structure and Mechanics, 1st ed. Princeton University Press, New Jersey, 2002.
[3] S.C. Cowin, L. Cardoso, Blood and interstitial flow in the hierarchical pore space architecture of bone tissue, J. Biomech. 48 (2015) 842–854, https://doi.org/10.1016/j.jbiomech.2014.12.013.
[4] J. Robles-Linares, E. Ramírez-Cedillo, H. Siller, C. Rodríguez, J. Martínez-López, Parametric Modeling of Biomimetic Cortical Bone Microstructure for Additive Manufacturing, Materials (Basel) 12 (2019) 913, https://doi.org/10.3390/ma12060913.
[5] N. Reznikov, M. Bilton, L. Lari, M.M. Stevens, R. Kröger, Fractal-like hierarchical organization of bone begins at the nanoscale, Science (80-.) 360 (2018) 1–10, https://doi.org/10.1126/science.aao2189.
[6] Z. Liao, D.A. Axinte, On monitoring chip formation, penetration depth and cutting malfunctions in bone micro-drilling via acoustic emission, J. Mater. Process. Technol. 229 (2016) 82–93, https://doi.org/10.1016/j.jmatprotec.2015.09.016.
[7] Z. Liao, D. Axinte, D. Gao, On modelling of cutting force and temperature in bone milling, J. Mater. Process. Technol. 266 (2019) 627–638, https://doi.org/10.1016/j.jmatprotec.2018.11.039.
[8] O. Gavalda Diaz, G. Garcia Luna, Z. Liao, D. Axinte, The new challenges of machining ceramic matrix composites (CMCs): review of surface integrity, Int. J. Mach. Tools Manuf. 139 (2019) 24–36, https://doi.org/10.1016/j.ijmachtools.2019.01.003.
[9] Z. Liao, A. Abdelhafeez, H. Li, Y. Yang, O.G. Diaz, D. Axinte, State-of-the-art of surface integrity in machining of metal matrix composites, Int. J. Mach. Tools Manuf. 143 (2019) 63–91, https://doi.org/10.1016/j.ijmachtools.2019.05.006.
[10] Z. Liao, D.A. Axinte, On chip formation mechanism in orthogonal cutting of bone, Int. J. Mach. Tools Manuf. 102 (2016) 41–55, https://doi.org/10.1016/j.ijmachtools.2015.12.004.
[11] Y. Zhang, L. Xu, C. Wang, Z. Chen, S. Han, B. Chen, J. Chen, Mechanical and thermal damage in cortical bone drilling in vivo, Proc. Inst. Mech. Eng. Part H J. Eng. Med. 233 (2019) 621–635, https://doi.org/10.1177/0954411919840194.
[12] A. Anesi, M. Ferretti, F. Cavani, R. Salvatori, M. Bianchi, A. Russo, L. Chiarini, C. Palumbo, Structural and ultrastructural analyses of bone regeneration in rabbit cranial osteotomy : Piezosurgery versus traditional osteotomes, J. Cranio-Maxillofacial Surg. 46 (2018) 107–118, https://doi.org/10.1016/j.jcms.2017.10.004.
[13] D. Taylor, J.A.N.G. Hazenberg, T.C. Lee, Living with cracks- damage and repair in human bone, Nat. Mater. 6 (2007) 263–268, https://doi.org/10.1038/nmat1866.
[14] N.M. Hancox, Biology of Bone, 1st ed. Cambridge University Press, Cambridge, 1972.
[15] B.S. Noble, The osteocyte lineage, Arch. Biochem. Biophys. 473 (2008) 106–111, https://doi.org/10.1016/j.abb.2008.04.009.
[16] M. Mediouni, T. Kucklick, S. Poncet, R. Madiouni, A. Abouaomar, H. Madry, M. Cucchiarini, B. Chopko, N. Vaughan, M. Arora, K. Gökkuş, M. Lozoya Lara, L. Paiva Cedeño, A. Volosnikov, M. Hesmati, K. Ho, An overview of thermal necrosis: present and future, Curr. Med. Res. Opin. 35 (2019) 1555–1562, https://doi.org/10.1080/03007995.2019.1603671.
[17] Z. Yang, L. Zhu, G. Zhang, C. Ni, B. Lin, Review of ultrasonic vibration-assisted machining in advanced materials, Int. J. Mach. Tools Manuf. 156 (2020) 103594, https://doi.org/10.1016/j.ijmachtools.2020.103594.
[18] R.D. Ventura, A.R. Padalhin, B.T. Lee, Functionalization of extracellular matrix (ECM) on multichannel biphasic calcium phosphate (BCP) granules for improved bone regeneration, Mater. Des. 192 (2020) 108653, https://doi.org/10.1016/j.matdes.2020.108653.
[19] U.T. Iwaniec, T.J. Wronski, R.T. Turner, Histological analysis of bone, in: J. Walker, J. Walker (Eds.), Methods Mol. Biol. Springer 2008, pp. 325–341, https://doi.org/10.1007/978-1-59745-242-7_21.
[20] B.B.G.M. Franssen, P.J. Diest, A.H. Schuurman, M. Kon, Drilling k-wires, what about the osteocytes? An experimental study in rabbits, Arch. Orthop. Trauma Surg. 128 (2008) 83–87, https://doi.org/10.1007/s00402-007-0382-z.
[21] F. Karaca, B. Aksakal, M. Kom, Influence of orthopaedic drilling parameters on temperature and histopathology of bovine tibia: an in vitro study, Med. Eng. Phys. 33 (2011) 1221–1227, https://doi.org/10.1016/j.medengphy.2011.05.013.
[22] Z. Liao, D.A. Axinte, D. Gao, A novel cutting tool design to avoid surface damage in bone machining, Int. J. Mach. Tools Manuf. 116 (2017) 52–59, https://doi.org/10.1016/j.ijmachtools.2017.01.003.
[23] L. Shu, S. Li, M. Terashima, W. Bai, T. Hanami, R. Hasegawa, N. Sugita, A novel self-centring drill bit design for low-trauma bone drilling, Int. J. Mach. Tools Manuf. 154 (2020) 103568, https://doi.org/10.1016/j.ijmachtools.2020.103568.
[24] J.M. Davis, M. Saei, D.P. Mohanty, A. Udupa, T. Sugihara, S. Chandrasekar, Cutting of tantalum: why it is so difficult and what can be done about it, Int. J. Mach. Tools Manuf. 157 (2020) 103607, https://doi.org/10.1016/j.ijmachtools.2020.103607.
[25] J.Y. Rho, T.Y. Tsui, G.M. Pharr, Elastic properties of human cortical and trabecular lamellar bone measured by nanoindentation, Biomaterials. 18 (1997) 1325–1330, https://doi.org/10.1016/S0142-9612(97)00073-2.
[26] J.Y. Rho, R.B. Ashman, C.H. Turner, Young's modulus of trabecular and cortical bone material: ultrasonic and microtensile measurements, J. Biomech. 26 (1993) 111–119, https://doi.org/10.1016/0021-9290(93)90042-D.
[27] A. Ascenzi, P. Baschieri, A. Benvenuti, The bending properties of single osteons, J. Biomech. 23 (1990) 763–771, https://doi.org/10.1016/0021-9290(90)90023-V.
[28] J.L. Kuhn, S.A. Goldstein, R. Choi, M. London, L.A. Feldkamp, L.S. Matthews, Comparison of the trabecular and cortical tissue moduli from human iliac crests, J. Orthop. Res. 7 (1989) 876–884, https://doi.org/10.1002/jor.1100070614.
[29] D. Kong, G. Lin, Y. Shi, Z. Gu, Y. Gao, Y. Feng, Performance of heterotopic bone elicited with bone morphogenic protein-2 microspheres as a bone repair material, Mater. Des. 191 (2020) 108657, https://doi.org/10.1016/j.matdes.2020.108657.
[30] O.A. Tertuliano, J.R. Greer, The nanocomposite nature of bone drives its strength and damage resistance, Nat. Mater. 15 (2016) 1195–1202, https://doi.org/10.1038/nmat4719.

[31] W.C. Oliver, G.M. Pharr, An improved technique for determining hardness and elastic modulus using load and displacement sensing indentation experiments, J. Mater. Res. 7 (1992) 1564–1583, https://doi.org/10.1557/JMR.1992.1564.
[32] J. Schwiedrzik, R. Raghavan, A. Bürki, V. LeNader, U. Wolfram, J. Michler, P. Zysset, In situ micropillar compression reveals superior strength and ductility but an absence of damage in lamellar bone, Nat. Mater. 13 (2014) 740–747, https://doi.org/10.1038/nmat3959.
[33] A.A. Poundarik, T. Diab, G.E. Sroga, A. Ural, A.L. Boskey, C.M. Gundberg, D. Vashishth, Dilatational band formation in bone, Proc. Natl. Acad. Sci. U. S. A. 109 (2012) 19178–19183, https://doi.org/10.1073/pnas.1201513109.
[34] A.A. Lloyd, B. Gludovatz, C. Riedel, E.A. Luengo, R. Saiyed, E. Marty, D.G. Lorich, J.M. Lane, R.O. Ritchie, B. Busse, E. Donnelly, Atypical fracture with long-term bisphosphonate therapy is associated with altered cortical composition and reduced fracture resistance, Proc. Natl. Acad. Sci. U. S. A. 114 (2017) 8722–8727, https://doi.org/10.1073/pnas.1704460114.
[35] A.J. Bushby, V.L. Ferguson, A. Boyde, Nanoindentation of bone: comparison of specimens tested in liquid and embedded in polymethylmethacrylate, J. Mater. Res. 19 (2004) 249–259, https://doi.org/10.1557/jmr.2004.19.1.249.
[36] J. Schwiedrzik, A. Taylor, D. Casari, U. Wolfram, P. Zysset, J. Michler, Nanoscale deformation mechanisms and yield properties of hydrated bone extracellular matrix, Acta Biomater. 60 (2017) 302–314, https://doi.org/10.1016/j.actbio.2017.07.030.
[37] J.X. Ma, W.W. He, J. Zhao, M.J. Kuang, H.H. Bai, L. Sun, B. Lu, A.X. Tian, Y. Wang, B.C. Dong, Y. Wang, X.L. Ma, Bone microarchitecture and biomechanics of the necrotic femoral head, Sci. Rep. 7 (2017) 1–10, https://doi.org/10.1038/s41598-017-13643-2.
[38] A. Varvani-Farahani, H. Najmi, A damage assessment model for cadaveric cortical bone subjected to fatigue cycles, Int. J. Fatigue 32 (2010) 420–427, https://doi.org/10.1016/j.ijfatigue.2009.08.002.
[39] G. Augustin, S. Davila, K. Mihoci, T. Udiljak, D.S. Vedrina, A. Antabak, Thermal osteonecrosis and bone drilling parameters revisited, Arch. Orthop. Trauma Surg. 128 (2008) 71–77, https://doi.org/10.1007/s00402-007-0427-3.
[40] M.A.K. Liebschner, Biomechanical considerations of animal models used in tissue engineering of bone, Biomaterials. 25 (2004) 1697–1714, https://doi.org/10.1016/S0142-9612(03)00515-5.
[41] A.I. Pearce, R.G. Richards, S. Milz, E. Schneider, S.G. Pearce, Animal models for implant biomaterial research in bone: a review, Eur. Cells Mater. 13 (2007) 1–10, https://doi.org/10.22203/eCM.v013a01.
[42] G. Zhang, X. Deng, F. Guan, Z. Bai, L. Cao, H. Mao, The effect of storage time in saline solution on the material properties of cortical bone tissue, Clin. Biomech. 57 (2018) 56–66, https://doi.org/10.1016/j.clinbiomech.2018.06.003.
[43] J.C.H. Goh, E.J. Ang, K. Bose, Effect of preservation medium on the mechanical properties of cat bones, Acta Orthop. 60 (1989) 465–467, https://doi.org/10.3109/17453678909149321.
[44] BSI Standards Publication, Metallic Materials - Instrumented indentation test of hardness and materials parameters. Part 4, Test method for metallic and non-metallic coatings (ISO 14577-4:2016) (2016) 2–4.
[45] K.J. Altman, Microscale Machining and Mechanical Characterization of Bone Tissue, The Ohio State University, 2009http://www.albayan.ae.
[46] M.D. Morris, G.S. Mandair, Raman assessment of bone quality, Clin. Orthop. Relat. Res. 469 (2011) 2160–2169, https://doi.org/10.1007/s11999-010-1692-y.
[47] C.H. Bachman, E.H. Ellis, Fluorescence of bone, Nature. 206 (1965) 1328–1331.
[48] I. Notingher, J.R. Jones, S. Verrier, I. Bisson, P. Embanga, P. Edwards, J.M. Polak, L.L. Hench, Application of FTIR and Raman spectroscopy to characterisation of bioactive materials and living cells, Spectroscopy. 17 (2003) 275–288, https://doi.org/10.1155/2003/893584.
[49] J.S. Yerramshetty, C. Lind, O. Akkus, The compositional and physicochemical homogeneity of male femoral cortex increases after the sixth decade, Bone. 39 (2006) 1236–1243, https://doi.org/10.1016/j.bone.2006.06.002.
[50] R.K. Pandey, S.S. Panda, Drilling of bone: a comprehensive review, J. Clin. Orthop. Trauma. 4 (2013) 15–30, https://doi.org/10.1016/j.jcot.2013.01.002.
[51] J.D. Bancroft, H.C. Cook, Manual of Histological Techniques and their Diagnostic Applications, 1st ed. Churchill Livingstone, London, 1994.
[52] W.W. Gerberich, J. Michler, W.M. Mook, R. Ghisleni, F. Östlund, D.D. Stauffer, R. Ballarini, Scale effects for strength, ductility, and toughness in “brittle” materials, J. Mater. Res. 24 (2009) 898–906, https://doi.org/10.1557/jmr.2009.0143.
[53] F. Östlund, P.R. Howie, R. Ghisleni, S. Korte, K. Leifer, W.J. Clegg, J. Michler, Ductile-brittle transition in micropillar compression of GaAs at room temperature, Philos. Mag. 91 (2011) 1190–1199, https://doi.org/10.1080/14786435.2010.509286.
[54] H. Zhang, B.E. Schuster, Q. Wei, K.T. Ramesh, The design of accurate micro-compression experiments, Scr. Mater. 54 (2006) 181–186, https://doi.org/10.1016/j.scriptamat.2005.06.043.
[55] M.F. Ashby, R.H. Jones, David, Engineering Materials, 4th ed.1, Butterworth-Heinemann, 2012.
[56] V. Gupta, P.M. Pandey, R.K. Gupta, A.R. Mridha, Rotary ultrasonic drilling on bone: a novel technique to put an end to thermal injury to bone, Proc. Inst. Mech. Eng. Part H J. Eng. Med. 231 (2017) 189–196, https://doi.org/10.1177/0954411916688500.
[57] D. Axinte, Y. Guo, Z. Liao, A.J. Shih, R. M'Saoubi, N. Sugita, Machining of biocompatible materials — recent advances, CIRP Ann. 68 (2019) 629–652, https://doi.org/10.1016/j.cirp.2019.05.003.
[58] A.P. Mamede, A.R. Vassalo, G. Piga, E. Cunha, S.F. Parker, M.P.M. Marques, L.A.E. Batista De Carvalho, D. Gonçalves, Potential of bioapatite hydroxyls for research on archeological burned bone, Anal. Chem. 90 (2018) 11556–11563, https://doi.org/10.1021/acs.analchem.8b02868.
[59] T.L. Anderson, Fracture Mechanics. Fundamentals and Applications, 4th ed. CRC Press, 2017.
[60] F. Östlund, K. Rzepiejewska-Malyska, K. Leifer, L.M. Hale, Y. Tang, R. Ballarini, W.W. Gerberich, J. Michler, Brittle-to-ductile transition in uniaxial compression of silicon pillars at room temperature, Adv. Funct. Mater. 19 (2009) 2439–2444, https://doi.org/10.1002/adfm.200900418.
[61] M. Granke, M.D. Does, J.S. Nyman, The role of water compartments in the material properties of cortical bone, Calcif. Tissue Int. 97 (2015) 292–307, https://doi.org/10.1007/s00223-015-9977-5.
[62] J. Samuel, J.S. Park, J. Almer, X. Wang, Effect of water on nanomechanics of bone is different between tension and compression, J. Mech. Behav. Biomed. Mater. 57 (2016) 128–138, https://doi.org/10.1016/j.jmbbm.2015.12.001.
[63] M. Maghsoudi-Ganjeh, X. Wang, X. Zeng, Computational investigation of the effect of water on the nanomechanical behavior of bone, J. Mech. Behav. Biomed. Mater. 101 (2020) 103454, https://doi.org/10.1016/j.jmbbm.2019.103454.
[64] M. Kate, S. Palaskar, P. Kapoor, Implant failure: a dentist's nightmare, J. Dent. Implant. 6 (2016) 51, https://doi.org/10.4103/0974-6781.202154.
[65] P. Christen, K. Ito, R. Ellouz, S. Boutroy, E. Sornay-Rendu, R.D. Chapurlat, B. Van Rietbergen, Bone remodelling in humans is load-driven but not lazy, Nat. Commun. 5 (2014)https://doi.org/10.1038/ncomms5855.